NH_3 condensation in a plate heat exchanger
Flow pattern based models of heat transfer and frictional pressure drop

Tao, Xuan; Infante Ferreira, Carlos

DOI
10.1016/j.ijheatmasstransfer.2020.119774

Publication date
2020

Document Version
Final published version

Published in
International Journal of Heat and Mass Transfer

International Journal of Heat and Mass Transfer 154 (2020) 119774

Contents lists available at ScienceDirect

International Journal of Heat and Mass Transfer

journal homepage: www.elsevier.com/locate/hmt

NH_3 condensation in a plate heat exchanger: Flow pattern based models of heat transfer and frictional pressure drop

Xuan Tao [a,*], Carlos A. Infante Ferreira [a]

[a] Process and Energy Laboratory, Delft University of Technology, Leeghwaterstraat 39, 2628 CB Delft, The Netherlands

ARTICLE INFO

Article history:
Received 27 January 2020
Revised 6 April 2020
Accepted 7 April 2020

Keywords:
Condensation mechanism
Heat transfer model based on flow pattern
Lockhart and Martinelli model
Separated flow
Plate heat exchanger
NH_3

ABSTRACT

This paper develops predicting models for NH_3 condensation in plate heat exchangers based on the experiments of flow patterns, heat transfer coefficients and frictional pressure drop previously reported by the authors. The aim is to provide design methods of compact plate condensers used in NH_3 systems, which are not available in open literature. The experimental data are firstly compared with selected correlations, showing a poor agreement. A heat transfer model is developed based on flow patterns, which represents the transition from convective condensation to gravity-controlled condensation. The physical interpretation of the two-phase multiplier approach and the deviation from Nusselt's theory are discussed. A transition criterion of condensation mechanisms is proposed based on the wetting characteristics. Since the flow patterns indicate separated flow, the Lockhart and Martinelli model is selected and is modified to predict the frictional pressure drop. The model is the sum of the liquid pressure drop, vapor pressure drop and interface pressure drop. The contributions of vapor pressure drop and interface pressure drop are discussed and quantified. The proposed heat transfer and frictional pressure drop models show good predictive performances. NH_3 flow has large two-phase slip because of the large density ratio. Plate heat exchangers have corrugated channels and tend to break up the liquid film. The models identify the distinct flow characteristics based on flow patterns.

1. Introduction

NH_3 is an environment friendly natural refrigerant with superior thermal properties. However, its application is restrained due to safety issues. Plate heat exchangers (PHEs) have the potential to be used in NH_3 systems such as for the recovery of low grade heat. The compact structures are able to transfer large heat loads with reduced charge of working fluid. Thus the safety risk can be mitigated. Furthermore, PHEs have the advantage of high thermal effectiveness and design flexibility, bringing about wide utilization in refrigeration, pharmacy and chemical engineering. PHEs consist of outside frame plates and inside stacked plates. Stacked plates usually have sinusoidal corrugations and provide heat transfer areas. Two adjacent plates form flow channels whose geometry and area change periodically [1,2].

Two-phase vertical downward flow in PHEs has been widely experimentally investigated, which is the common flow direction of condensers and absorbers [3–5]. Tao et al. [2] reviewed the condensation mechanisms in PHEs. The transition from gravity-controlled condensation to convective condensation is determined by mass fluxes and vapor qualities. Larger mass fluxes promote convective condensation. Furthermore, the fluid properties play important roles. The flow tends to be separated when the two-phase density ratio is large, and is close to homogeneous flow with small density ratio. Condensation pressures, inlet superheating, plate geometries and temperature driving forces also influence the heat transfer and frictional pressure drop [2].

Tao and Infante Ferreira [6] reviewed the heat transfer and frictional pressure drop correlations for condensation in PHEs. An experimental database is developed including 2376 heat transfer data and 1590 frictional pressure drop data. The working fluids are HFCs, hydrocarbons, HFOs and CO_2, but NH_3 is not included. Most correlations have been derived from experimental data, and are applicable in the original and similar operating ranges. In order to be assessed in larger ranges, these correlations have been compared with the experimental database. The heat transfer correlations of Longo et al. [4] and Kuo et al. [7] predict the experimental data best. A new correlation is proposed for frictional pressure drop [6].

Experimental data of NH_3 condensation in PHEs are scarce, and details of the experiments are missing in old papers [8,9]. Re-

* Corresponding Author.
E-mail addresses: x.tao@tudelft.nl (X. Tao), c.a.infanteferreira@tudelft.nl (C.A.I. Ferreira).

https://doi.org/10.1016/j.ijheatmasstransfer.2020.119774

Nomenclature

Symbols

Co	Convection number [-]
d	Diameter [m]
d_h	Hydraulic diameter [m]
f	Darcy friction factor [-]
Fr	Froude number [-]
g	Gravitational constant [ms^{-2}]
G	Mass flux [kg m^{-2} s^{-1}]
h	Enthalpy [J kg^{-1}]
j_G	Non-dimensional gas velocity Eq. (1) [-]
L_p	Port-to-port plate length [m]
P	Pressure [Pa]
Pr	Prandtl number [-]
Re	Reynolds number [-]
T	Temperature [°C]
v	Superficial velocity [ms^{-1}]
We	Weber number [-]
x	Vapor quality [-]
X	Lockhart-Martinelli parameter [-]

Greek symbols

α	Heat transfer coefficient [W m^{-2} K^{-1}]
β	Chevron angle to flow direction [°]
Δ	Difference [-]
ε	Void fraction [-]
ϕ_L	Two-phase multiplier [-]
Θ	Fraction of convective condensation in Eq. (16) [-]
λ	Thermal conductivity [W m^{-1} K^{-1}]
μ	Dynamic viscosity [Pas]
ρ	Density [kg m^{-3}]
σ	Surface tension [N m^{-1}]

Subscripts

av	Averaged
c	Combined condensation
cc	Convective condensation
cr	Critical condition
exp	Experimental data
G	Gas or vapor
gc	Gravity-controlled condensation
GO	Gas or vapor only
int	At two-phase interface
L	Liquid
LG	Latent liquid to vapor
ll	Laminar-laminar flow
LO	Liquid only
$LT1$	Limit 1 in Eq. (8)
$LT2$	Limit 2 in Eq. (9)
pre	Predicted data
sat	At saturation conditions
TP	Two-phase
T	Transition value
tt	Turbulent-turbulent flow
$wall$	At wall conditions

cently, the authors experimentally investigated the flow patterns, heat transfer coefficients (HTCs) and frictional pressure drop [10]. NH_3 has distinct fluid properties from HFCs and hydrocarbons. NH_3 is characterized by large two-phase density ratio, thermal conductivity, surface tension and latent heat. Consequently, the experimental HTCs and frictional pressure drop show sharp sensitivity to the vapor qualities [10]. To the best of the authors' knowledge, no correlation has been specially proposed for NH_3 condensation in PHEs. In tubes, the correlations derived from HFCs or hydrocarbons mismatch the experimental data of NH_3 [11,12]. The accuracy of cross calculation is unknown in PHEs. This work investigates NH_3 condensation in PHEs. Derived from experimental data [10], this paper develops heat transfer and frictional pressure drop models based on flow patterns. The primary physical processes are described, while the flow details cannot be quantified and are considered by involving empirical constants.

2. Previous physically based modeling of condensation

During condensation in tubes, the theory of heat transfer and frictional pressure drop has been established to describe the physical process of two-phase flow. The theoretical researches on PHEs are limited, and the geometric influence is not thoroughly understood. This Section reviews the previous studies that are used as the starting points to develop the predicting models.

2.1. Heat transfer models based on flow patterns

During the condensation in horizontal tubes, flow pattern based heat transfer models have been recognized to be accurate and widely applicable. Annular flow is modelled as fully convective condensation. Stratified flow is considered to combine gravity-controlled condensation at the top of the tube and convective condensation at the bottom, and gravity-controlled condensation is usually dominant. Slug and churn flows fall into these two regimes and are not analyzed separately. Bubbly flow only takes place at large mass fluxes, which go beyond the general operating ranges of condensation [13–16]. Some papers used different terms, but the physical interpretation is similar [17].

Dobson and Chato [14] experimentally analyzed the reliance of HTCs on flow patterns. The flow patterns are classified into gravity-controlled flow and shear-controlled flow. In gravity-controlled regime, HTCs are sensitive to temperature driving force but are almost independent of mass fluxes. The HTCs of shear-controlled flow are characterized by the significant influences of mass fluxes and vapor qualities. These authors proposed mechanistic models for the two regimes.

Thome et al. [16] assumed uniform liquid film thickness for annular flow. The film thickness is calculated using a void fraction model. Convective condensation takes place during annular flow. For stratified flow, the film is considered as a part of the annular ring located at the bottom, where convective condensation prevails. The wall is unwetted at the top, where the Nusselt theory is applied. The portions of the two condensation mechanisms are determined by stratified angles. In order to predict NH_3 in-tube (8 mm diameter) condensation, Park and Hrnjak [12] kept the flow pattern map and condensation mechanisms of El Hajal et al. [15] and Thome et al. [16], but modified the heat transfer correlations.

Cavallini et al. [13] divided the condensation mechanisms according to the dependence on temperature driving force. Temperature driving force independent regime is equivalent to convective condensation, while temperature driving force dependent regime is similar to gravity-controlled condensation. In Eq. (1), j_G is the non-dimensional gas velocity. When j_G is larger than the transition value in Eq. (2), convective condensation applies. C_T depends on the working fluids. 1.6 is recommended for hydrocarbons, while 2.6 applies for other fluids such as HFCs, NH_3, CO_2 and H_2O. At smaller values of j_G, the HTC combines convective condensation and Nusselt correlations. Fronk and Garimella [11,18] developed a heat transfer model for NH_3 condensation in small diameter tubes (0.98, 1.44 and 2.16 mm). They also used j_G as the transition criterion. During annular flow, the heat transfer is enhanced by the interfacial roughness arising from two-phase momentum difference.

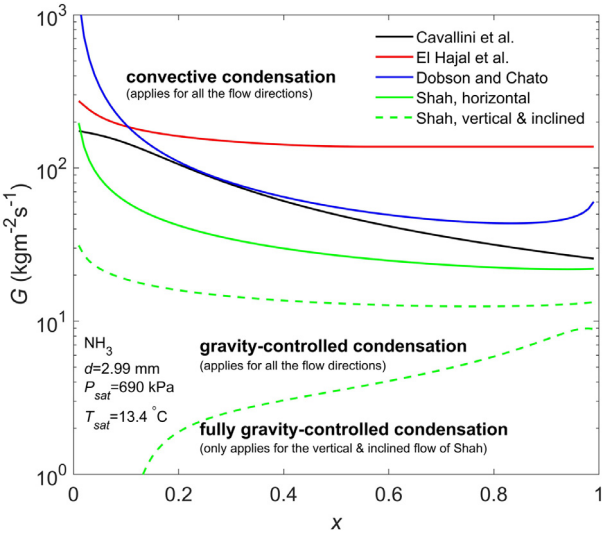

Fig. 1. Transition of condensation mechanisms. The criteria of Cavallini et al. [13], El Hajal et al. [15] and Dobson and Chato [14] were developed for horizontal tubes. Shah [17] included horizontal, vertical and inclined tubes.

The correlations of Cavallini et al. [13] were recommended for non-annular flow.

$$j_G = \frac{xG}{[gd_h\rho_G(\rho_L-\rho_G)]^{0.5}} \tag{1}$$

$$j_{G,T} = \left[\left(\frac{7.5}{4.3\left(\left(\frac{\mu_L}{\mu_G}\right)^{0.1}\left(\frac{\rho_G}{\rho_L}\right)^{0.5}\left(\frac{1-x}{x}\right)^{0.9}\right)^{1.11}+1}\right)^{-3}+C_T^{-3}\right]^{-0.333} \tag{2}$$

The above models have been proposed for horizontal flow. Shah [17] specified the influence of flow directions. During horizontal flow, condensation mechanisms were divided into convective condensation and gravity-controlled condensation. Fully gravity-controlled condensation is only included for vertical and inclined flow. The difference between gravity-controlled condensation and fully gravity-controlled condensation is the convection effect. For gravity-controlled condensation, convection still contributes to heat transfer. The convection attenuates during fully gravity-controlled condensation. Instead of analyzing flow patterns, Shah [17] developed the heat transfer models by fitting a large number of experimental data.

Fig. 1 shows several transition lines. Dobson and Chato [14] used Soliman's modified Froude number to distinguish stratified flow from annular flow. The transition generally happens at higher vapor quality for small mass fluxes. El Hajal et al. [15] differentiated stratified flow and annular or intermittent flow using the void fraction and stratified angle. Stratified flow includes fully-stratified flow and stratified-wavy flow, whose difference results from the occurrence of waves at the two-phase interface. These two sub-flow patterns are considered the same in terms of condensation mechanisms. Cavallini et al. [13] classified the condensation mechanisms by referring to Eqs. (1)–(2). The variation of HTCs is gradual during transition. According to Shah [17], vertical and inclined flows have smaller transition mass fluxes than horizontal flow. Fully gravity-controlled condensation only happens at small mass fluxes and high vapor qualities for vertical and inclined flow, where little condensate accumulates at the bottom of the tubes and convection is negligible.

2.2. Frictional pressure drop models based on flow patterns

Two-phase flow is divided into homogeneous flow and separated flow. The homogeneous model assumes the two-phase velocities are the same, and the flow is considered as an equivalent fluid. Bubbly flow and mist flow are generally categorized as homogeneous flow. According to the separated flow model, vapor velocity is larger than liquid mainly because of the density ratio. Separated flow includes stratified flow and annular flow.

The separated flow model calculates the two-phase frictional pressure drop by summing the liquid pressure drop, vapor pressure drop and the pressure drop at the interface. Lockhart and Martinelli [19] analyzed separated flow by assuming the static pressure drops of liquid and vapor are the same. This assumption applies to space unchanged flow patterns and excludes intermittent flow. Chisholm [20] developed the theoretical basis of this model and specified the interfacial shear force. According to the theoretical assumption, the liquid and vapor streams have the same flow mechanisms during two-phase flow as single-phase flow. Homogeneous flow is a special case of this model with zero slip and uniform density. In this case, the experimental data are generally over-predicted.

Friedel [21] claimed that the frictional pressure drop depends on the flow direction because the slip at the two-phase interface is different. Under gravity, liquid moves faster vertically downward, resulting in larger void fraction or smaller slip ratio. One correlation was proposed for horizontal and vertically upward flow, while another one was developed for vertically downward flow. Additionally, surface tension affects the frictional pressure drop by acting on the two-phase interface.

Müller-Steinhagen and Heck [22] analyzed the sensitivity of frictional pressure drop with vapor qualities, and observed a peak value for $x \approx 0.85$. At higher vapor qualities, the frictional pressure drop decreases as a smaller amount of liquid reduces the interfacial shear force. A correlation was developed and was compared with others. This correlation satisfactorily predicted the experimental database which is mainly composed of air-water and steam-water. The homogeneous correlations were only applicable for low vapor qualities, while Lockhart and Martinelli [19] model generally over-predicted the experimental data.

During NH_3 condensation in a tube (8 mm diameter), Park and Hrnjak [12] recommended the models of Friedel [21] and Müller–Steinhagen and Heck [22] for the range above 1 kPa m^{-1}, which were predicted to be intermittent or annular flow. For values below 1 kPa m^{-1}, the homogeneous model had better performance. Under these conditions stratified flow was expected to occur. It is separated flow, but the two-phase velocity difference is small because of the small mass fluxes. Fronk and Garimella [23] measured the frictional pressure drop during NH_3 condensation inside a small diameter tube (1.44 mm). The experimental data were under-predicted by the Friedel [21] model for about 30%. The deviation is mainly attributed to the large surface tension of NH_3.

Fig. 2 compares the separated flow models. The trends of these models are similar. With increasing vapor qualities, the two-phase pressure drop increases at low and intermediate values, and then decreases when approaching pure vapor. The maximum two-phase pressure drop is between $x = 0.8$ and $x = 0.9$. The changes of the liquid and vapor pressure drop are monotonic. Vapor pressure drop is much larger than liquid pressure drop because the two-phase densities and viscosities of NH_3 differ dramatically. The interfacial pressure drop is larger at intermediate vapor qualities when both phases play roles.

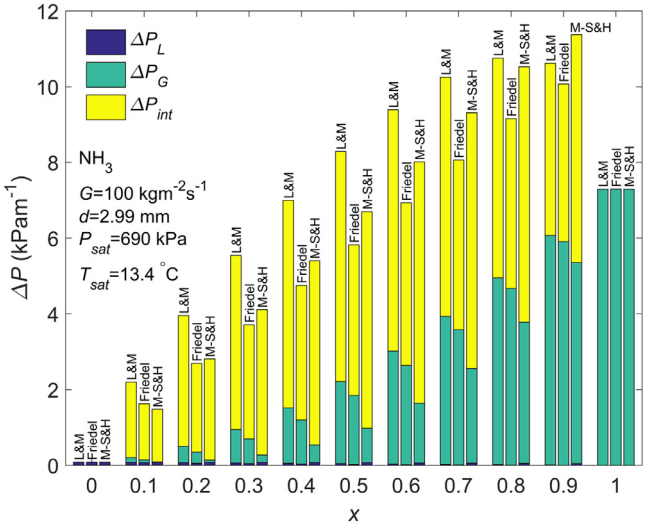

Fig. 2. Comparison of models by dividing the two-phase pressure drop into the liquid pressure drop, vapor pressure drop and the pressure drop at the interface. The separated models are Lockhart and Martinelli [19] model (L&M) [20], Friedel [21] model and Müller–Steinhagen and Heck [22] model (M-S&H). The single-phase correlation is from Kast et al. [49].

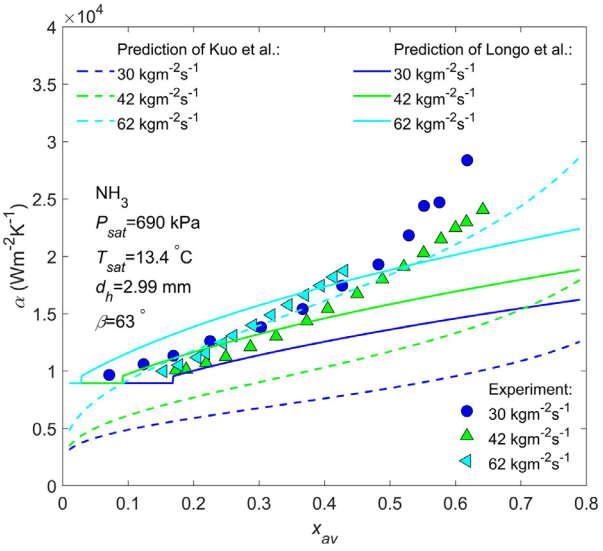

Fig. 3. Condensation HTCs of NH_3 with varying averaged vapor quality and mass fluxes. Comparison of experimental and predicted data. The prediction is from Longo et al. [4] (solid lines) and Kuo et al. [7] (dashed lines).

3. Comparison with existing correlations

The authors have reported experimental HTCs and frictional pressure drops of NH_3 condensation in a PHE [10]. The experiments cover the mass fluxes of 21–78 kg m^{-2} s^{-1}, the averaged vapor qualities of 0.05–0.65 and the saturated pressure of 630–930 kPa. In the tested ranges, the flow patterns are full film flow and partial film flow. HTCs increase significantly with vapor qualities and are less sensitive to mass fluxes. Frictional pressure drop increases sharply with both vapor qualities and mass fluxes. The HTCs and frictional pressure drop show the characteristics of separated flow. The flow patterns result from the fluid properties of NH_3. The experimental data are compared with selected correlations in this Section. The comparison is presented in terms of mass fluxes and vapor qualities.

3.1. Heat transfer correlations

Tao and Infante Ferreira [6] summarized condensation heat transfer correlations in PHEs and developed an extensive experimental database. Eight correlations have been assessed by comparing with the database. The correlations of Longo et al. [4] and Kuo et al. [7] show the best performance. Nevertheless, NH_3 is not included in the database.

Fig. 3 compares these two correlations with the experimental data for three mass fluxes. Kuo et al. [7]'s correlation is a two-phase multiplier approach, which assumes annular flow [24]. The condensation heat transfer is similar to the convective heat transfer of liquid phase since all the heat is transferred through the liquid [24]. The vapor flow and heat flux enhance the heat transfer and are considered as a two-phase multiplier. According to this correlation, HTCs increase significantly with the vapor quality, agreeing with the trend of the experimental data.

The correlation of Longo et al. [4] is composed of convective condensation and gravity-controlled condensation. The convective correlation involves the equivalent Reynolds number, which treats the two-phase flow as a single equivalent fluid. The vapor flow is replaced with an additional liquid flow by keeping the same shear force at the two-phase interface. The conversion ratio depends on the two-phase density ratio [25]. The sensitivity to the vapor quality is less noticeable than for the experimental data. Convective condensation is transformed into gravity-controlled condensation at low vapor qualities, and the HTCs become insensitive to mass fluxes and vapor qualities.

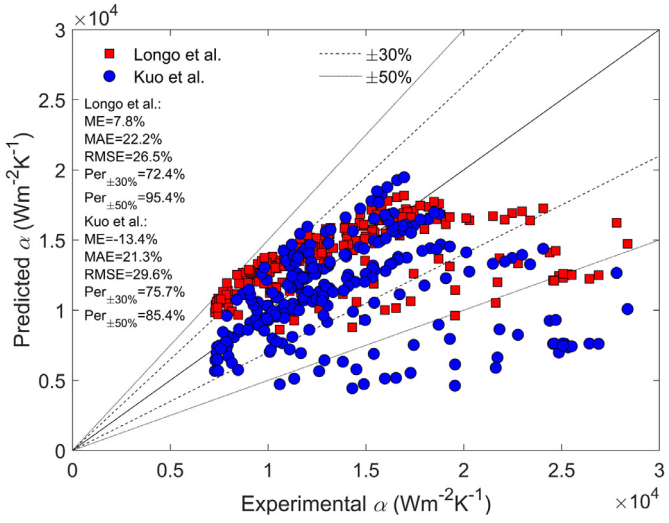

Fig. 4. Comparison of NH_3 condensation HTCs with correlations. Mean error (ME): $\frac{1}{n}\sum_1^n \frac{\alpha_{pre}-\alpha_{exp}}{\alpha_{exp}}$; Mean absolute error (MAE): $\frac{1}{n}\sum_1^n \frac{|\alpha_{pre}-\alpha_{exp}|}{\alpha_{exp}}$; Root mean squared error (RMSE): $\sqrt{\frac{1}{n}\sum_1^n \left(\frac{\alpha_{pre}-\alpha_{exp}}{\alpha_{exp}}\right)^2}$; *Per* $_{\pm 30\%}$: Percentage of experimental data within ± 30%; *Per* $_{\pm 50\%}$: Percentage of experimental data within ± 50%.

Fig. 4 presents the accuracy of the correlations. The correlation of Kuo et al. [7] predicts 75.7% of the experimental data within ±30%. The mean absolute error (MAE) is 21.3%. It estimates correctly the significant sensitivity to vapor qualities and shows consistent trend with the experimental data. Nevertheless, predicted data of different mass fluxes are separated. This correlation is more accurate for intermediate and large mass fluxes, and dramatically under-predicts the data of small mass fluxes. Longo et al. [4]'s correlation predicts 72.4% of the data within ±30%. It over-predicts the experimental HTCs at low vapor qualities, and under-predicts the experimental HTCs at high vapor qualities. The predicted values of large and intermediate mass fluxes converge, but the under-prediction for small mass flux is noticeable. In short, the correla-

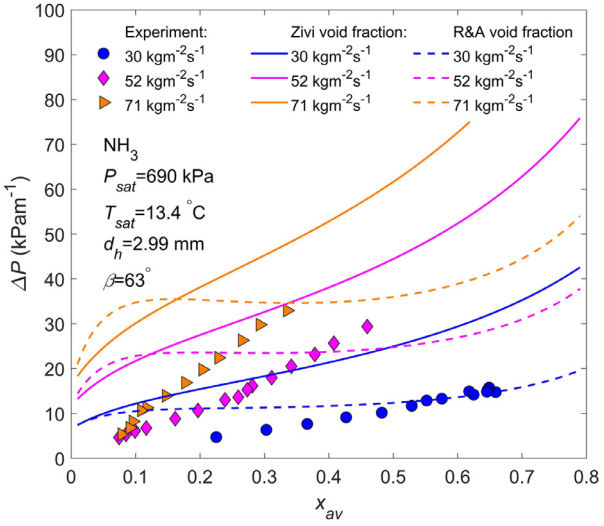

Fig. 5. Frictional pressure drop of NH_3 with varying averaged vapor quality and mass fluxes. Comparison of experimental and predicted data. The prediction is from Tao and Infante Ferreira [6] and is based on the void fraction of Zivi [33] (solid lines) and Rouhani and Axelsson [34] (R&A) (dashed lines).

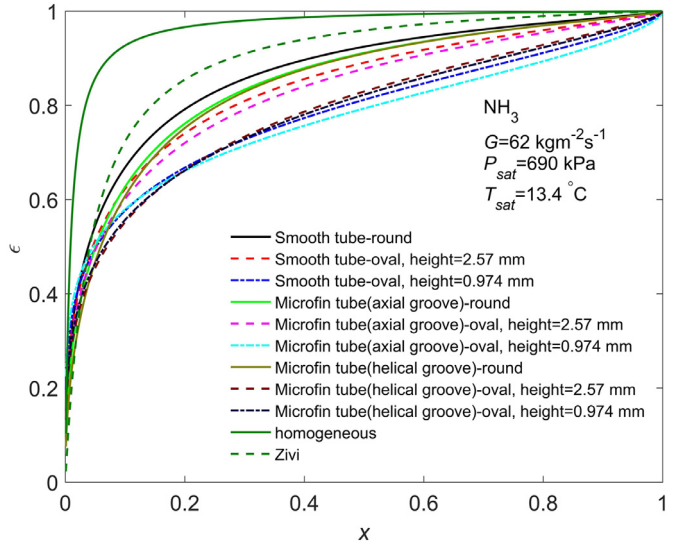

Fig. 6. Influence of geometrical structure on void fraction. Round tubes and oval tubes with and without microfins are compared. The oval tubes with 0.974 mm height are flatter than those with 2.57 mm (adapted from [35]).

tion of Kuo et al. [7] over-estimates the influence of mass fluxes, while Longo et al. [4]'s correlation cannot predict the sharp sensitivity to vapor qualities.

3.2. Two-phase Fanning friction factor combined with void fraction

Tao and Infante Ferreira [6] also assessed six frictional pressure drop correlations with an experimental database, including two-phase Fanning friction factor and Lockhart–Martinelli model. The agreement of the correlations is poor, and a new correlation has been developed. In the previous researches of PHEs, Lockhart–Martinelli's model is mostly chosen for air-water flow [26–28]. The air-water system is characterized by a large two-phase density ratio, and separated flow patterns such as full film flow and partial film flow cover large ranges [2]. The database is mostly composed of HFCs, hydrocarbons and HFOs, whose two-phase density ratio is relatively small [6]. Nino et al. [29] and Adams et al. [30] suggested the homogeneous void fraction for fluids of small liquid-vapor density ratio and separated void fraction for large density ratio. The new correlation assumes homogeneous flow and calculates the two-phase Fanning friction factor. When applied for NH_3, this correlation significantly over-predicts the experimental data [31]. The two-phase slip ratio of NH_3 is much larger than 1. The homogeneous void fraction over estimates the averaged velocity and thus the shear force. Jassim et al. [32] proposed to calculate the averaged density using the separated void fraction model.

The visualization experiments indicate that the NH_3 flow is separated [10]. To the best of the authors' knowledge, no void fraction model is specially developed for PHEs. Tao et al. [31] compared several void fraction models originally proposed for microchannels. In Fig. 5, the models of Zivi [33] and Rouhani and Axelsson [34] are used to calculate the averaged density. Zivi [33] proposed a theoretical model and claimed to provide the lower limit of void fraction. Rouhani and Axelsson's [34] model was originally derived for flow boiling, and is more suitable for low pressure. This model is chosen because the condensation in this paper happens at relatively low pressure.

According to Fig. 5, both prediction methods show larger values than the experimental data. The possible reason is that the estimated void fraction is larger than the actual values in PHEs. At low vapor qualities, the prediction based on Zivi [33] void fraction has deviations larger than three times. The slope of the lines based on Rouhani and Axelsson's [34] void fraction becomes flat at intermediate vapor qualities. The flow passage of PHEs is approximately rectangular, and the ratio of width to length is small. The channel has a corrugated structure and is interrupted by the contact points of adjacent plates. The void fraction is different from what applies for smooth channels. Liquid is likely to be held at the corner of the flow passages and at the contact points, which reduces the liquid velocity and increases the slip ratio. The void fraction consequently decreases. Fig. 6 shows the void fraction calculated by Wilson et al. [35]'s model, which indicates the geometry influence by comparing round tubes and oval tubes with and without microfins. The void fraction in oval tubes is lower than in round tubes. The oval tubes are flatter for smaller heights and have lower void fraction. Microfin tubes have generally lower void fraction than smooth tubes. The void fraction of smooth-round tubes is close to Zivi [33] model, while the micro-fins and oval structures reduce the void fraction. Moreover, in Fig. 5, the experimental data increase sharply with vapor qualities, which is different from the trend of the predictions. As shown in Fig. 2, the sharp increase is a characteristic of separated flow.

Although the calculation proposed by Tao and Infante Ferreira [6] has been derived from an extensive experimental database, the application is limited to the working fluids covered by the database (HFCs, hydrocarbons and HFOs), which are characterized by small two-phase density ratio and tend to stream in homogeneous flow. Triplett et al. [36] concluded that the homogeneous model predicted correctly the frictional pressure drop of bubbly and slug flow, but significantly over-estimated the data of annular flow. The flow of NH_3 is separated. The frictional pressure drop needs to be analyzed making use of a different approach.

4. Development of a heat transfer model

This Section firstly develops a heat transfer correlation for convective condensation, and then establishes the transition criterion of condensation mechanisms depending on the wetting characteristics. A heat transfer correlation for combined condensation is also developed, and is composed of convective condensation and gravity-controlled condensation. The experimental data reported in Tao et al. [10] are used as the basis for these correlations.

4.1. Convective condensation

During NH_3 condensation in a PHE, the flow patterns are full film flow and partial film flow below 100 kg m^{-2} s^{-1} [10]. For full film flow, the wall surface is completely wetted by the liquid. Full film flow is equivalent to annular flow in tubes, but the liquid cannot develop a regular ring around the plate surface due to the corrugated flow passages. The interaction between the vapor in the core and the liquid around it gives rise to convective condensation.

All the heat is transferred through the liquid film, where the heat transfer process is similar to single-phase flow. Vapor phase shaves the two-phase interface and enhances the heat transfer. The two-phase multiplier approach was originally developed for annular flow in tubes and is applicable for the full film flow in PHEs [24]. The two-phase multiplier depends on the vapor flow and two-phase fluid properties. It generally has the form of Eq. (3). α_{cc} is the HTC of convective condensation. α_L is the liquid HTC and only identifies the liquid mass flux. It is calculated using the liquid Reynolds number, Re_L. In Eq. (4), the liquid only HTC, α_{LO}, assumes all the fluid is liquid and is determined according to VDI [1]. f_{LO} is the Darcy friction factor and is calculated in Eqs. (8)–(10) [1]. This equation is derived from a large range of geometrical parameters and agrees well with the water HTCs determined previously by the authors [37,10]. Eq. (5) shows the difference between α_L and α_{LO}. f_L/f_{LO} is approximately 1 especially for large chevron angles. Eqs. (6)–(7) calculate Re_{LO} and Re_L.

$$\alpha_{cc} = \alpha_L F(x, \rho_L/\rho_G, G) \tag{3}$$

$$\alpha_{LO} = 0.122(f_{LO}\sin 2\beta)^{0.374}\mathrm{Re}_{LO}^{0.748}\mathrm{Pr}_L^{0.333}\left(\frac{\mu}{\mu_{wall}}\right)^{0.167}\frac{\lambda_L}{d_h} \tag{4}$$

$$\begin{aligned}\alpha_L &= 0.122(f_L\sin 2\beta)^{0.374}\mathrm{Re}_L^{0.748}\,\mathrm{Pr}_L^{0.333}\left(\tfrac{\mu}{\mu_{wall}}\right)^{0.167}\tfrac{\lambda_L}{d_h}\\ &= \alpha_{LO}\left(\tfrac{f_L}{f_{LO}}\right)^{0.374}(1-x)^{0.748} \approx \alpha_{LO}(1-x)^{0.748}\end{aligned} \tag{5}$$

$$Re_{LO} = \frac{Gd_h}{\mu_L} \tag{6}$$

$$Re_L = \frac{G_L d_h}{\mu_L} = \frac{G(1-x)d_h}{\mu_L} \tag{7}$$

$$f_{LT1} = \begin{cases} 64\mathrm{Re}^{-1}, & \mathrm{Re} < 2000 \\ (1.8\lg(\mathrm{Re}) - 1.5)^{-2}, & \mathrm{Re} \geq 2000 \end{cases} \tag{8}$$

$$f_{LT2} = \begin{cases} 3.8\left(597\mathrm{Re}^{-1} + 3.85\right), & \mathrm{Re} < 2000 \\ 3.8\left(39\mathrm{Re}^{-0.289}\right), & \mathrm{Re} \geq 2000 \end{cases} \tag{9}$$

$$f = \left(\frac{\cos\beta}{\sqrt{0.18\tan\beta + 0.36\sin\beta + f_{LT1}/\cos\beta}} + \frac{1-\cos\beta}{\sqrt{f_{LT2}}}\right)^{-2} \tag{10}$$

In order to confine the experimental data to fully developed convective condensation, only data with G_L > 40 kg m^{-2} s^{-1} are included to develop the correlation. Eq. (11) is obtained by multivariable regression analysis. The first term of the two-phase multiplier interprets the enhancement contributed by the vapor flow. It approaches 0 when x is 0, indicating that the enhancement vanishes as the fluid becomes liquid only. In Eq. (12), Co is the convection number and represents the slip velocity at the two-phase interface. As the reduced pressure increases, the two-phase properties become alike and the density ratio is close to 1, suppressing the slip at the interface. In Eq. (13), the liquid Froude number, Fr_L, is the ratio of inertia to gravity, and indicates the dominance of momentum effect or stratifying effect for separated flow. The second term in the bracket of Eq. (11) specifies the difference between

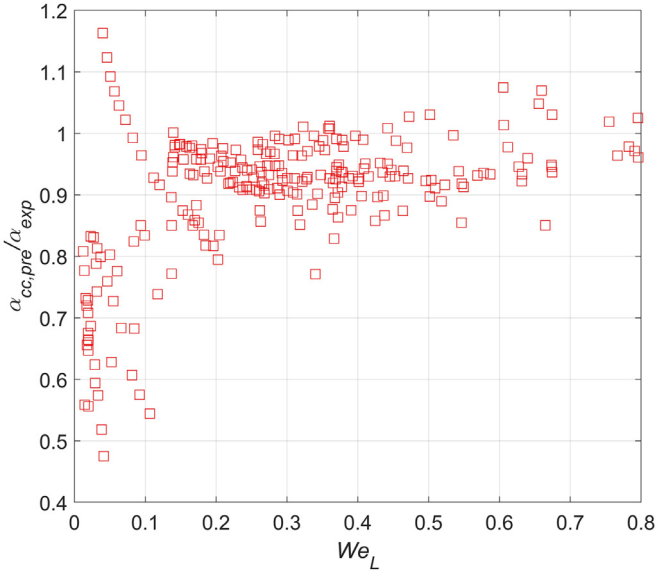

Fig. 7. Applicability of the correlation of convective condensation (Eq. (11)) in terms of We_L.

α_{LO} and α_L. α_{cc} becomes α_{LO} when the flow is single-phase liquid.

$$\alpha_{cc} = \alpha_{LO}\left(0.17Co^{-1.12}Fr_L^{-0.2} + (1-x)^{0.748}\right) \tag{11}$$

$$Co = \left(\frac{\rho_G}{\rho_L}\right)^{0.5}\left(\frac{1-x}{x}\right)^{0.8} \tag{12}$$

$$Fr_L = \frac{G^2}{\rho_L{}^2 g d_h} \tag{13}$$

The previous analysis is restricted to the data with G_L > 40 kg m^{-2} s^{-1}. Convective condensation extends to lower liquid mass fluxes. In small diameter channels, the magnitude of surface tension becomes prominent relative to gravity and shear force. Larger surface tension promotes the change from annular flow to wavy flow in tubes [38]. The surface tension affects the wetting characteristics and condensation mechanisms, while the inertial force tends to distribute the liquid film around the wall surface. In Eq. (14), the liquid Weber number, We_L, is the ratio of liquid inertia to surface tension. We_L is used to distinguish the condensation mechanisms. Eq. (11) is used to predict all the experimental data, and the comparison is presented in Fig. 7. When We_L > 0.12, the experimental data are well predicted, and the deviation is within ±20%. As We_L < 0.12, the experimental data are under predicted. Another condensation mechanism is involved, which enhances the heat transfer. The value of $We_{L,T} = 0.12$ is the transition criterion of condensation mechanisms.

$$We_L = \frac{\rho_L v_L^2 d_h}{\sigma} = \frac{G^2(1-x)^2 d_h}{\rho_L \sigma} \tag{14}$$

The transition line is presented in Fig. 8, which agrees well with the change of flow patterns. As compared with Fig. 1, the transition mass flux is smaller than in horizontal tubes, but is close to the value for vertical and inclined tubes. The flow direction affects the transition of condensation mechanisms because of the interaction between gravity and shear force. For fully gravity-controlled condensation, the condensate film formed on the wall flows almost vertically downward. By contrast, interfacial shear force dominates for convective condensation. The condensate film is less affected by gravity and flows along the main flow direction. The transition depends on the relative magnitudes of gravity and shear force.

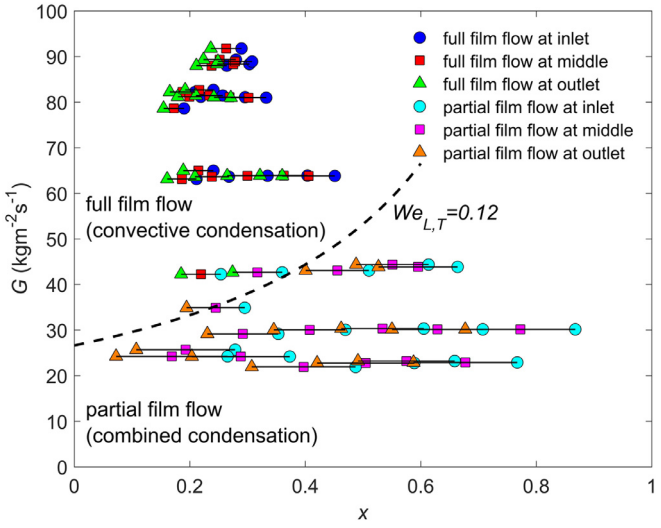

Fig. 8. Comparison of the flow pattern map with the criterion of condensation mechanisms ($We_{L,T} = 0.12$).

The flow in the corrugated groove of PHEs is similar to inclined downward flow in tubes [10]. The gravity is divided into the directions parallel to the groove and perpendicular to the groove [39]. Gravity supplements the shear force and has reduced stratifying effect. Consequently, convective condensation is promoted for inclined downward flow.

The transition happens at higher vapor quality for large mass fluxes. This trend of the transition line is different from Fig. 1. The criterion of PHEs is based on the wetting characteristics, while the criteria of tubes are mainly derived from j_G. The possible reason is the difference in channel geometries. The velocity distribution is not uniform within the flow section. The velocity is larger at the center and becomes smaller close to the wall. The vapor has a larger velocity than the liquid. The vapor with large inertia pushes the liquid radially. In circular tubes, the force is nearly uniform in circumferential direction, and liquid tends to reside on the wall uniformly. Larger vapor mass fluxes enhance the inertia effect so as to overcome the stratifying effect. PHEs have irregular flow section, and the ratio of width to length is small. The liquid is pushed by the vapor in all directions. The corrugated surface breaks up the liquid film and distributes the broken droplets randomly. Consequently, a certain amount of liquid is required to completely wet the wall. Larger liquid mass fluxes also promote the waviness of the film flow and change the flow patterns.

In PHEs, the transition mass fluxes of other refrigerants are smaller than for NH_3. According to Longo et al. [4], the transition mass fluxes are about 20 kg $m^{-2}s^{-1}$ for HFCs and HFOs (R134a, R410A, R236fa, R1234yf, R1234ze(E)), and are around 15 kg m^{-2} s^{-1} for hydrocarbons (R600a, R290, R1270). Mancin et al. [40] stated that the transition values are around 20 kg m^{-2} s^{-1} for R410A and R407C. Thonon and Bontemps [41] identified the transition mass fluxes as 5–13 kg m^{-2} s^{-1} for R601, R600 and R290. These experiments were conducted at small mass fluxes, and the HTCs of gravity-controlled condensation are larger than convective condensation. Zhang et al. [42] concluded that the transition mass fluxes are about 20 kg m^{-2} s^{-1} for R134a and R1234ze(E). Sarraf et al. [43] reported condensation of R601 in the range of 9–30 kg m^{-2} s^{-1}. Gradual transition happens at 10–20 kg m^{-2} s^{-1} and relies on the vapor qualities. The difference can be attributed to the surface tension. NH_3 has larger surface tension and reduces the wettability. The mass flux needs to be larger for complete wetting. Consequently, gravity-controlled condensation extends to larger mass fluxes.

4.2. Combined condensation

During the visualization experiments of NH_3 condensation in a PHE [10], the flow direction of the fluid is observed to be a combination of crossing flow and wavy longitudinal flow. The flow in grooves is inclined downward. As the liquid mass fluxes decrease, a part of the wall surface is not wetted. The flow pattern becomes partial film, and some vapor is in contact with the wall directly. Partial film flow is similar to stratified flow in tubes. The condensation deviates from convective condensation and shows similarity to gravity-controlled condensation. Convective condensation occurs in the wetted area. In the dry zones, the condensation is similar to the Nusselt's theory except for the influence of shear force. The vapor phase exerts shear force on the thin condensate film and enhances the heat transfer [44]. In Eq. (15), the heat transfer correlation combines convective condensation, α_{cc}, with gravity-controlled condensation, α_{gc}. Θ is the fraction of convective condensation. Because the overall heat transfer area is only contributed by these two mechanisms, the fraction of gravity-controlled condensation can be determined as $1-\Theta$.

$$\alpha_c = \Theta\alpha_{cc} + (1-\Theta)\alpha_{gc} \tag{15}$$

The flow pattern changes gradually from full film flow to partial film flow, and the HTC of convective condensation is identified to be the same as given by Eq. (11). Θ needs to be determined before calculating the gravity-controlled condensation. During the condensation in horizontal tubes, for stratified flow, Dobson and Chato [14] and Thome et al. [16] estimated the fraction of gravity-controlled condensation by using the wetted angle. Cavallini et al. [13] used j_G to quantify the fraction of gravity-controlled condensation. In PHEs, the wetted angle is difficult to measure. As shown in Eq. (16), Θ is determined to be the ratio of liquid Weber number to the transition liquid Weber number. The fraction of the wetted area increases with the liquid mass flux [45], and Eq. (15) approaches convective condensation.

$$\Theta = We_L/We_{L,T} \tag{16}$$

In Eq. (17), the Nusselt correlation is kept as the starting point [46]. The original Nusselt correlation is based on several assumptions. The deviations from the assumptions have minor influences, or the resulting overprediction and underprediction partly offset each other. Consequently, the correlation is applicable in wide ranges of conditions [47]. Nevertheless, most of the complicating factors in the confined channels enhance heat transfer, and thus the influences need to be identified. The film thickness reduces when the vapor shaves the interface. The vapor flow accelerates the condensate film and generates waves, contributing to film convection. Pr_L indicates the relative importance of convection and conduction. Co is included to interpret the enhancement contributed by two-phase slip, and the constants are obtained by fitting the data.

$$\alpha_{gc} = 0.36Co^{-0.28}\left[\frac{g\rho_L(\rho_L-\rho_G)\Delta h_{LG}\lambda_L^3}{\mu_L\Delta T d_h}\right]^{0.25} Pr_L^{0.333} \tag{17}$$

4.3. Assessment of heat transfer model

Fig. 9 compares the proposed heat transfer model with the experimental data from Tao et al. [10]. 96.3% of the experimental data are predicted within ±20%. The MAE is 7.4%. The data are composed of convective condensation and combined condensation. This model predicts accurately the noticeable sensitivity to vapor qualities and moderate sensitivity to mass fluxes.

Tao and Infante Ferreira [6] developed an extensive experimental database of condensation in PHEs. The database is mostly composed of HFCs, hydrocarbons and HFOs, which usually have

Table. 1
Two-phase fluid properties of typical refrigerants at $T_{sat} = 20\ ^{\circ}C$[a]

Units	P_{sat} kPa	P_{sat}/P_{cr} -	ρ_G kg•m^{-3}	ρ_L kg•m^{-3}	μ_G μPa•s	μ_L μPa•s	Δh_{LG} kJ•kg^{-1}	σ mN•m^{-1}	λ_L W•m^{-1}K^{-1}	Pr_L -
NH_3	857	0.075	6.70	610	9.69	134	1186	21.7	0.481	1.32
R601	57	0.017	1.72	626	6.61	230	370	16.0	0.114	4.64
R600a	302	0.083	7.91	557	7.36	159	334	10.6	0.091	4.20
R600	208	0.055	5.31	579	7.21	167	367	12.5	0.107	3.78
R290	836	0.197	18.08	500	8.01	102	344	7.6	0.096	2.84
R134a	572	0.141	27.78	1225	11.49	207	182	8.7	0.083	3.50
R410A	1447	0.295	56.80	1083	13.33	126	194	6.0	0.092	2.27
R1234ze(E)	427	0.118	22.61	1179	11.92	203	171	9.6	0.076	3.66
Air/water	857[b]	-	10.22	999	18.32	1001	-	72.8[c]	0.598	7.00

[a] The fluid properties are calculated using Refprop [55]
[b] This is not the saturated pressure, but the pressure used to determine the fluid properties of mixture
[c] The surface tension of mixture is calculated using Vargaftik et al. [56]

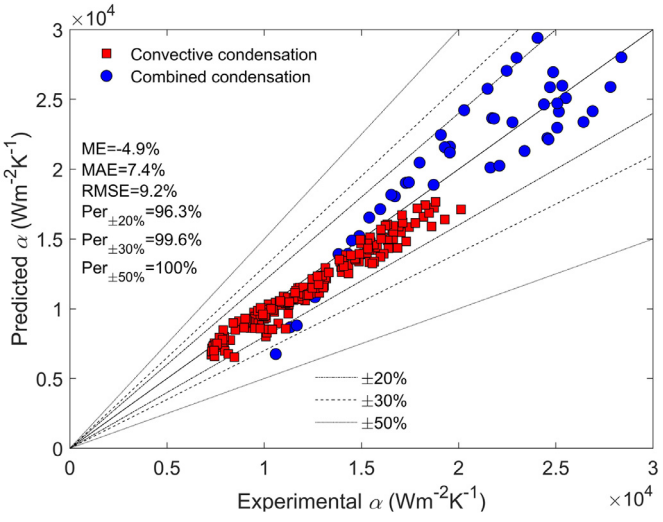

Fig. 9. Comparison of NH_3 condensation HTCs with the proposed model. Mean error (ME): $\frac{1}{n}\sum_1^n \frac{\alpha_{pre}-\alpha_{exp}}{\alpha_{exp}}$; Mean absolute error (MAE): $\frac{1}{n}\sum_1^n \frac{|\alpha_{pre}-\alpha_{exp}|}{\alpha_{exp}}$; Root mean squared error (RMSE): $\sqrt{\frac{1}{n}\sum_1^n (\frac{\alpha_{pre}-\alpha_{exp}}{\alpha_{exp}})^2}$; $Per_{\pm 20\%}$: Percentage of experimental data within ± 20%; $Per_{\pm 30\%}$: Percentage of experimental data within ± 30%; $Per_{\pm 50\%}$: Percentage of experimental data within ± 50%.

much smaller two-phase density ratio than NH_3. Table 1 gives the fluid properties of typical refrigerants and air/water mixture. R601, R600a and R600 also have large two-phase density ratio, and are used to validate the proposed heat transfer correlations.

Sarraf et al. [43] measured the local HTCs during R601 condensation in a PHE, and the experimental data are presented in Fig. 10(a). HTCs increase sharply with vapor qualities, and are less sensitive to mass fluxes. Larger mass fluxes slightly reduce the HTCs at low vapor qualities, and have greater influences at high vapor qualities. The model predicts well the trends of vapor qualities. Because of the large two-phase density ratio, a slight rise of the vapor qualities greatly intensifies the shear force and enhances the heat transfer. According to the proposed model, the shear force is weak at low vapor qualities. Larger mass fluxes promote full film flow. Increased wetted areas reinforce the liquid film, which serves as heat transfer resistance. The scatter is larger at high vapor qualities. The model is derived from data limited to low and intermediate vapor qualities. Moreover, the measurement at high vapor qualities has large uncertainties. Larger HTCs reduce the heat transfer difference and enlarge the relative uncertainty for given sensor accuracy. Fortunately, because of the small heat transfer resistance, the heat transfer areas corresponding to high vapor qualities account for a small portion of PHEs, which brings about limited design uncertainty.

Longo [48] and Thonon and Bontemps [41] measured the overall HTCs during the complete condensation of R600a, R600 and R601. Fig. 10(b) and (c) compare the experimental data with prediction. The averaged vapor quality is the integrated mean value of the whole condenser. Shah [24] argued that the averaged vapor quality is closer to 0.4 than 0.5. Larger mass fluxes have minor influences on HTCs, which is the compensating effect of larger shear force and thicker liquid film. The model is more accurate at large mass fluxes, but overpredicts the experimental data at small mass fluxes.

In summary, the model can be extended from NH_3 to other refrigerants of large two-phase density ratio. The model is applicable to the vapor qualities of 0–0.8 and the mass fluxes of 20–80 kg m^{-2} s^{-1}. Application to higher vapor qualities and smaller mass fluxes should be with concern. The foremost PHE geometries are hydraulic diameters and chevron angles, which generally span the range of 3–8 mm and 25°–70°, respectively [6]. The heat transfer model is a two-phase multiplier approach. The involved single-phase correlation identifies geometric parameters [1]. The model is expected to apply to most commercial chevron PHEs with standard geometries. The influence of saturated pressure is mainly attributed to vapor density, liquid thermal conductivity and latent heat. The model is suitable for low reduced pressure.

Fig. 11 shows a sensitivity analysis according to the proposed heat transfer model, indicating a sharp increase with vapor qualities. In Fig. 11(a), the condensation mechanism is combined condensation at 20 kg m^{-2} s^{-1} since the wall cannot be completely wetted. At larger mass fluxes, convective condensation applies at low vapor qualities and changes into combined condensation with increasing vapor qualities. Combined condensation takes place when part of the wall becomes dry. The transition vapor quality is higher for larger mass fluxes. When the condensation mechanism remains the same, HTCs increase with mass fluxes. It applies for both combined condensation at high vapor qualities and convective condensation at low vapor qualities. For lower vapor qualities, the HTCs at 20 kg m^{-2} s^{-1} are larger because the earlier transition to combined condensation. Fig. 11(b) shows the influence of saturated pressures. The HTCs are slightly larger for lower condensation pressures. The larger two-phase density ratio and viscosity difference intensify the shear force. Additionally, the thermal conductivity of liquid is larger for low pressures. The condensation mechanism changes close to the vapor quality of 0.4. Lower pressures slightly reduce the transition vapor quality.

5. Development of frictional pressure drop model

The frictional pressure drop is less affected by the transition of condensation mechanisms. Thus a unified model is developed in this Section. The original Lockhart–Martinelli model is firstly presented, and then is modified to identify the influence of surface

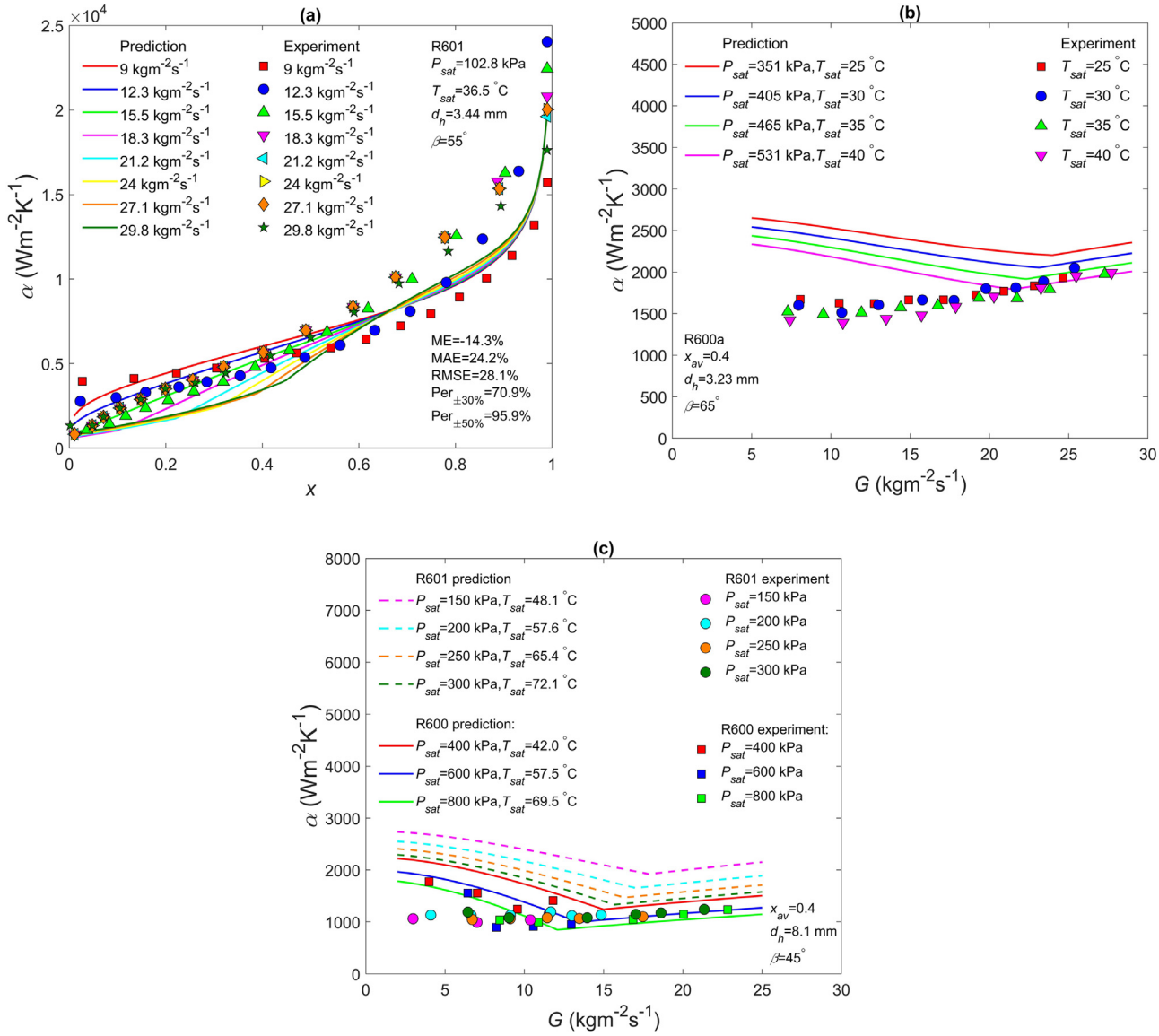

Fig. 10. Validation of the new heat transfer model, Eqs. (11) and (15)–(17), with the experimental data of (a) Sarraf et al. [43], (b) Longo [48], (c) Thonon and Bontemps [41].

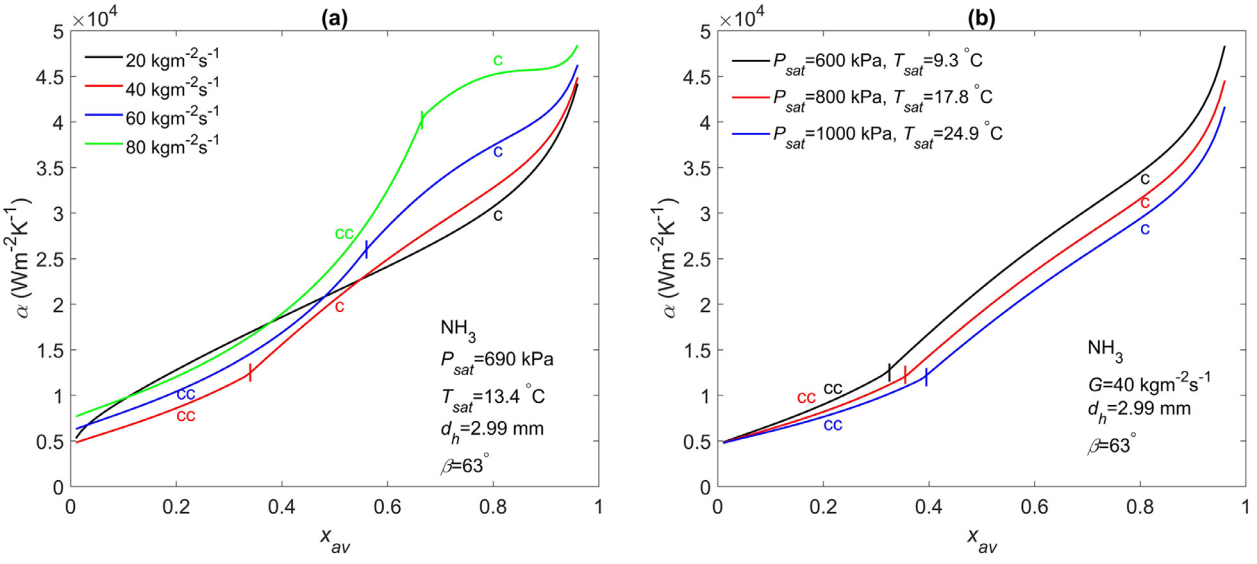

Fig. 11. Sensitivity of the HTCs to vapor qualities for (a) different mass fluxes, (b) different condensation pressures. cc: convective condensation, c: combined condensation.

tension and the contribution of the vapor pressure drop. The experimental data reported in Tao et al. [10] are used as the basis for this modified approach.

5.1. Separated flow model

Both full film flow and partial film flow are separated two-phase flows. The vapor phase has larger velocity than the liquid phase. The two-phase frictional pressure drop is the sum of the liquid pressure drop, vapor pressure drop and interface pressure drop. Lockhart–Martinelli model is selected as the starting point to predict the frictional pressure drop.

The original Lockhart–Martinelli model was developed for tubes and has the form of Eqs. (18)–(24) [20,19]. X is the ratio of the liquid to vapor pressure drops. X determines the contributions of liquid and vapor pressure drops. The value of X depends on whether the liquid and vapor are laminar or turbulent. Eqs. (21)–(22) apply to turbulent-turbulent flow and laminar-laminar flow based on the single-phase pressure drop correlations in tubes [49]. X is a function of vapor qualities and two-phase fluid properties. The ratios of densities and viscosities determine the two-phase slip at the interface. Eq. (18) can be converted into Eq. (25) by substituting Eqs. (19)–(20).

$$\phi_L^2 = 1 + \frac{C}{X} + \frac{1}{X^2} \tag{18}$$

$$\phi_L^2 = \frac{\Delta P_{TP}}{\Delta P_L} \tag{19}$$

$$X^2 = \frac{\Delta P_L}{\Delta P_G} = \frac{f_L}{f_G}\left(\frac{1-x}{x}\right)^2 \frac{\rho_G}{\rho_L} \tag{20}$$

$$X_{tt} = \left(\frac{1-x}{x}\right)^{0.875}\left(\frac{\rho_G}{\rho_L}\right)^{0.5}\left(\frac{\mu_L}{\mu_G}\right)^{0.125} \tag{21}$$

$$X_{ll} = \left(\frac{1-x}{x}\right)^{0.5}\left(\frac{\rho_G}{\rho_L}\right)^{0.5}\left(\frac{\mu_L}{\mu_G}\right)^{0.5} \tag{22}$$

$$\Delta P_L = f_L \frac{G_L^2}{2\rho_L}\frac{L_p}{d_h} = f_L \frac{G^2(1-x)^2}{2\rho_L}\frac{L_p}{d_h} \tag{23}$$

$$\Delta P_G = f_G \frac{G_G^2}{2\rho_G}\frac{L_p}{d_h} = f_G \frac{G^2 x^2}{2\rho_G}\frac{L_p}{d_h} \tag{24}$$

$$\Delta P_{TP} = \underbrace{\Delta P_L}_{\text{liqud pressure drop}} + \underbrace{C\sqrt{\Delta P_L \Delta P_G}}_{\text{interface pressure drop}} + \underbrace{\Delta P_G}_{\text{vapor pressure drop}} \tag{25}$$

In PHEs, the ratio of f cannot be easily represented by vapor quality and fluid properties like tubes in Eqs. (21)–(22). As shown in Eqs. (8)–(10), f_L and f_G are calculated based on single-phase flow correlations. It is recommended to calculate X according to Eq. (20) or calculate ΔP_{TP} directly using Eq. (25). The interface pressure drop is proportional to the geometric mean of the liquid and vapor pressure drops. The two-phase frictional pressure drop approaches the liquid or vapor pressure drop when x is 0 or 1, respectively. The interface pressure drop vanishes as the fluid becomes single phase.

During two-phase flow, the Lockhart and Martinelli model assumes that the vapor flow mechanism stays the same as for single-phase flow [20]. As shown in Fig. 2, the vapor pressure drop is predicted to be larger than the prediction of other models. Müller-Steinhagen and Heck [22] proposed the model introduced in Eq. (26), where ΔP_{LO} and ΔP_{GO} are the liquid only and vapor only pressure drops, respectively. This model is limited by the liquid and vapor pressure drops when the fluid becomes single phase. In order to be compared with Lockhart-Martinelli model, it is converted into Eq. (27). For fluids with large two-phase density ratio, the vapor pressure drop contributes primarily to the overall pressure drop. The Lockhart-Martinelli model involves the vapor pressure drop directly, while the model of Müller-Steinhagen and Heck reduces the contribution by multiplying with $(f_{GO}/f_G)x$. In PHEs, the single-phase frictional pressure drop identifies the influence of corrugated flow passages and has large values because of the geometry induced momentum dissipation [1]. The direct inclusion of vapor pressure drop over-predicts the two-phase pressure drop. The proposed model is presented in Eqs. (28)–(29). The contribution of the vapor pressure drop is modified and is proportional to the vapor quality.

$$\Delta P_{TP} = (1-x)^{1/3}\Delta P_{LO} + 2x(1-x)^{1/3}(\Delta P_{GO} - \Delta P_{LO}) + x^3 \Delta P_{GO} \tag{26}$$

$$\Delta P_{TP} = \underbrace{\frac{f_{LO}}{f_L}(1-x)^{-5/3}\Delta P_L}_{\text{liqud pressure drop}} + \underbrace{2x(1-x)^{1/3}(\Delta P_{GO} - \Delta P_{LO})}_{\text{interface pressure drop}} + \underbrace{\frac{f_{GO}}{f_G}x\Delta P_G}_{\text{vapor pressure drop}} \tag{27}$$

The original Lockhart–Martinelli model was reported to over-predict the frictional pressure drop when the surface tension becomes dominant [50,51]. Larger surface tension reduces the wetted area and flow resistance contributed by the large viscosity of the liquid phase [52]. Surface tension tends to smooth the two-phase interface and reduce the pressure drop [51]. The friction at the two-phase interface depends on flow patterns, and the Lockhart–Martinelli model should be modified accordingly [53]. Lower values of C are recommended when surface tension dominates at small diameter channels. In Eqs. (28)–(29), C is selected to be 2. Eq. (29) is obtained by substituting Eqs. (19)–(20) into Eq. (28). The single-phase pressure drop is calculated using the friction factor obtained from Eqs. (8)–(10). The two-phase frictional pressure drop is limited by single-phase pressure drop when the flow becomes liquid or vapor.

$$\phi_L^2 = 1 + \frac{2}{X} + \frac{x}{X^2} \tag{28}$$

$$\Delta P_{TP} = \underbrace{\Delta P_L}_{\text{liqud pressure drop}} + \underbrace{2\sqrt{\Delta P_L \Delta P_G}}_{\text{interface pressure drop}} + \underbrace{x\Delta P_G}_{\text{vapor pressure drop}} \tag{29}$$

5.2. Assessment of frictional pressure drop model

In Fig. 12, the proposed frictional pressure drop model predicts 73.8% of the experimental data within ±20%. The MAE is 14.6%. The data are divided into full film flow and partial film flow according to $We_{L,T} = 0.12$, which correspond to convective condensation and combined condensation, respectively. The experimental data of partial film flow are slightly over-predicted. For partial film flow, parts of the wall are sheared by the vapor instead of liquid, and the overall flow resistance is reduced. Moreover, the shear force at the two-phase interface is reduced since the interface shrinks and the vapor contacts the wall directly.

In Table 1, the two-phase fluid properties of air-water are similar to those of NH_3 with large density ratio and surface tension. The flow characteristics are expected to be similar. According to the experimental results of Tribbe and Müller-Steinhagen [54] and Winkelmann [28], the frictional pressure drop increases linearly

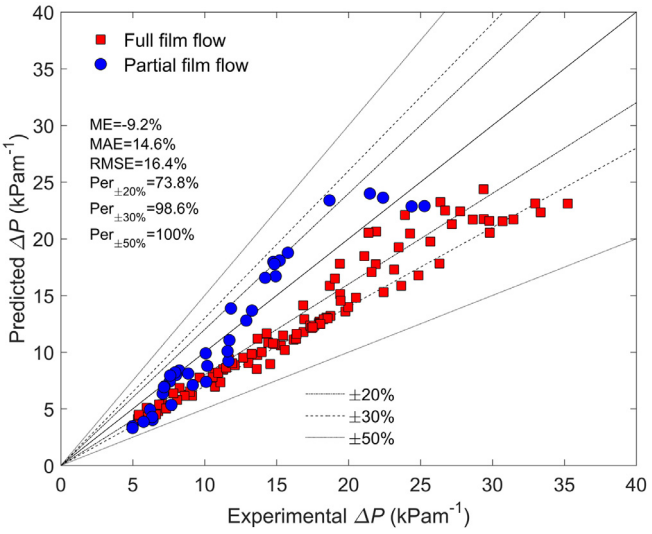

Fig. 12. Comparison of NH_3 frictional pressure drop with the present model. Mean error (ME): $\frac{1}{n}\sum_1^n \frac{\Delta P_{pre}-\Delta P_{exp}}{\Delta P_{exp}}$; Mean absolute error (MAE): $\frac{1}{n}\sum_1^n \frac{|\Delta P_{pre}-\Delta P_{exp}|}{\Delta P_{exp}}$; Root mean squared error (RMSE): $\sqrt{\frac{1}{n}\sum_1^n \left(\frac{\Delta P_{pre}-\Delta P_{exp}}{\Delta P_{exp}}\right)^2}$; $Per_{\pm 20\%}$: Percentage of experimental data within ± 20%; $Per_{\pm 30\%}$: Percentage of experimental data within ± 30%; $Per_{\pm 50\%}$: Percentage of experimental data within ± 50%.

with the vapor quality, which is the mass flow ratio of air to water. No maximum value exists at the region of high vapor qualities as shown in Fig. 2. The two-phase pressure drop is the sum of three components. In tubes with smooth surface, the liquid and vapor pressure drops are limited, while the interface pressure drop is noticeable because of the sags and crests. The maximum pressure drop results from the shear force at the two-phase interface. The corrugated channels of PHEs significantly intensify the single-phase pressure drop [1]. Bumpy two-phase interface is unlikely to further aggravate the momentum dissipation superposed to the wall friction. The interface pressure drop becomes secondary. Thus the two-phase pressure drop is proportional to vapor qualities. These data cannot be used to validate the proposed model because the operating conditions are not reported [54,28].

The model is limited to two-phase NH_3 flow. It is expected to cover the vapor qualities of 0–1 and the mass fluxes of 20–80 kg m^{-2} s^{-1}. Experimental data at high vapor qualities are not obtained. But the model approaches vapor only pressure drop with increasing vapor qualities, which agrees with physical interpretation. Similar to the proposed heat transfer model, the pressure drop model appears to be applicable to most commercial chevron PHEs and low reduced pressure. The sensitivity to geometric parameters is included in the single-phase correlations [1].

Fig. 13 presents the sensitivity of frictional pressure drop calculated from the proposed model. The frictional pressure drop increases dramatically with vapor qualities as the vapor phase occupies a larger portion of the flow section. In Fig. 13(a), larger mass fluxes increase the frictional pressure drop significantly and contribute to a later transition of flow patterns in terms of vapor qualities. As shown in Fig. 13(b), the saturated pressure has a minor influence at low vapor qualities where the frictional pressure drop is mainly contributed by the liquid phase. Higher saturated pressure has larger vapor density and reduces the volume flux significantly at high vapor qualities. Thus the slip and shear force between phases decrease.

6. Conclusions

This paper analyzes the wetting characteristics and interfacial properties of two-phase flow patterns during NH_3 condensation in PHEs. Based on the analysis, heat transfer and frictional pressure drop models are derived from the experimental data presented in a previous paper of the authors [10].

- The heat transfer model is presented in Eqs. (11) and (15)–(17). It distinguishes convective condensation and combined condensation. Convective condensation happens for full film flow, and a two-phase multiplier correlation has been developed. Combined condensation takes place for partial film flow. The heat transfer is composed of convective condensation and gravity-controlled condensation. The HTCs of gravity-controlled condensation deviate from Nusselt's theory because of the two-phase shear force and liquid convection. The transition criterion of condensation mechanisms is $We_{L,T} = 0.12$. A cross validation shows that the model is applicable for other refrigerants of similar fluid properties to NH_3.
- A unified model of separated flow is developed for frictional pressure drop, which is shown in Eqs. (28)–(29). The Lockhart and Martinelli model is modified to identify the reduction of vapor pressure drop and the influence of surface tension on the interface pressure drop.

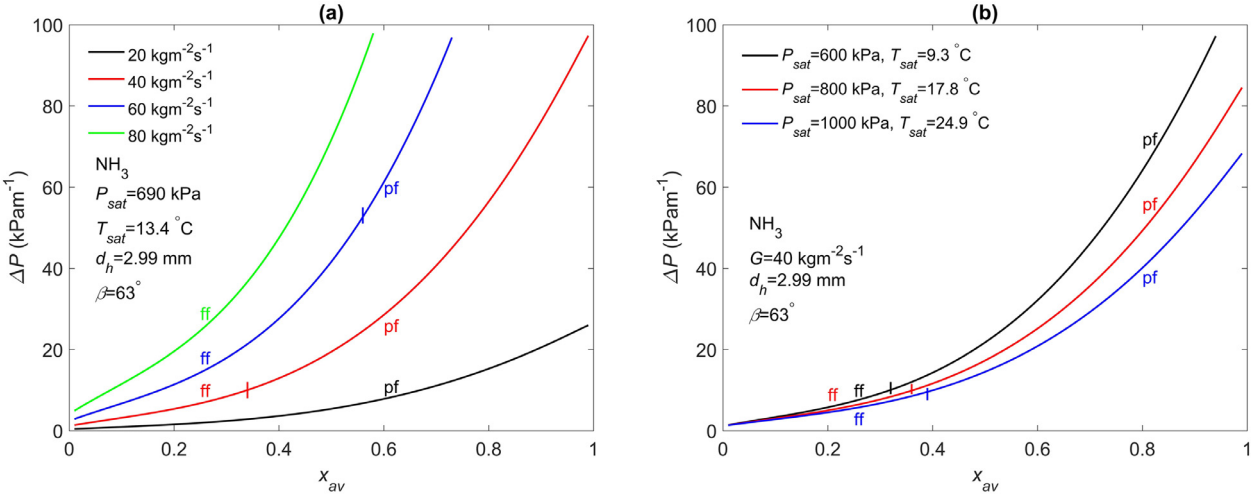

Fig. 13. Sensitivity of the frictional pressure drop with vapor qualities for (a) different mass fluxes, (b) different condensation pressure. ff: full film flow, pf: partial film flow.

Declaration of Competing Interest

The authors declare that they have no known competing financial interests or personal relationships that could have appeared to influence the work reported in this paper.

CRediT authorship contribution statement

Xuan Tao: Conceptualization, Methodology, Formal analysis, Investigation, Data curation, Visualization, Writing - original draft. **Carlos A. Infante Ferreira:** Conceptualization, Resources, Project administration, Funding acquisition, Methodology, Writing - review & editing, Supervision.

Acknowledgments

This project has been developed in cooperation with Allseas Engineering B.V. The authors acknowledge the financial support from the China Scholarship Council and from the Koude Groep Delft / Wageningen.

References

[1] H. Martin, Pressure drop and heat transfer in plate heat exchangers, in: P. Stephan, H. Martin, S. Kabelac, D. Mewes, M. Kind, K. Schaber (Eds.), VDI Heat Atlas, Springer, Dusseldorf, 2010, pp. 1516–1521. 2nd Edition.
[2] X. Tao, M.P. Nuijten, C.A Infante Ferreira, Two-phase vertical downward flow in plate heat exchangers: flow patterns and condensation mechanisms, Int. J. Refrig. 85 (2018) 489–510.
[3] S. Buscher, Visualization and modelling of flow pattern transitions in a cross–corrugated plate heat exchanger channel with uniform two-phase distribution, Int. J. Heat Mass Transf. 144 (2019) 118643.
[4] G.A. Longo, G. Righetti, C. Zilio, A new computational procedure for refrigerant condensation inside herringbone-type brazed plate heat exchanger, Int. J. Heat Mass Transf. 82 (2015) 530–536.
[5] F. Táboas, M. Vallès, M. Bourouis, A. Coronas, Flow boiling heat transfer of ammonia/water mixture in a plate heat exchanger, Int. J. Refrig. 33 (2010) 695–705.
[6] X. Tao, C.A Infante Ferreira, Heat transfer and frictional pressure drop during condensation in plate heat exchangers: assessment of correlations and a new method, Int. J. Heat Mass Transf. 135 (2019) 996–1012.
[7] W.S. Kuo, Y.M. Lie, Y.Y. Hsieh, T.F. Lin, Condensation heat transfer and pressure drop of refrigerant R-410A flow in a vertical plate heat exchanger, Int. J. Heat Mass Transf. 48 (25) (2005) 5205–5220.
[8] H. Kumar, in: The Design of Plate Heat Exchangers for Refrigerants, Proceedings of Institute of Refrigeration., London, The UK, 1992, pp. 50–55.
[9] C.B. Panchal, T.J. Rabas, Thermal performance of advanced heat exchangers for ammonia refrigeration systems, Heat Transf. Eng. 14 (1993) 42–57.
[10] X. Tao, E. Dahlgren, M. Leichsenring, C.A Infante Ferreira, NH3 condensation in a plate heat exchanger: Experimental investigation on flow patterns, heat transfer and frictional pressure drop, Int. J. Heat Mass Transf. 151 (2020) 119374.
[11] B.M. Fronk, S. Garimella, Condensation of ammonia and high-temperature-glide ammonia/water zeotropic mixtures in minichannels–part I: measurements, Int. J. Heat Mass Transf. 101 (2016) 1343–1356.
[12] C.Y. Park, P. Hrnjak, NH3 in-tube condensation heat transfer and pressure drop in a smooth tube, Int. J. Refrigeration. 31 (2008) 643–651.
[13] A. Cavallini, D.D. Col, L. Doretti, M. Matkovic, L. Rossetto, C Zilio, G Censi, Condensation in horizontal smooth tubes: a new heat transfer model for heat exchanger design, Heat Transfer Eng. 27 (2006) 31–38.
[14] M.K. Dobson, J.C. Chato, Condensation in smooth horizontal tubes, ASME J. Heat Transf. 120 (1998) 193–213.
[15] J.E. Hajal, J.R. Thome, A. Cavallini, Condensation in horizontal tubes, part 1: two-phase flow pattern map, Int. J. Heat Mass Transf. 46 (2003) 3349–3363.
[16] J.R. Thome, J. El Hajal, A. Cavallini, Condensation in horizontal tubes, part 2: new heat transfer model based on flow regimes, Int. J. Heat Mass Transf. 46 (2003) 3365–3387.
[17] M.M. Shah, An improved and extended general correlation for heat transfer during condensation in plain tubes, HVAC&R Res. 15 (2009) 889–913.
[18] B.M. Fronk, S. Garimella, Condensation of ammonia and high-temperature-glide ammonia/water zeotropic mixtures in minichannels–part II: heat transfer models, Int. J. Heat Mass Transf. 101 (2016) 1357–1373.
[19] R.W. Lockhart, R.C. Martinelli, Proposed correlation of data for isothermal two-phase, two-component flow in pipes, Chem. Eng. Prog. 45 (1949) 39–48.
[20] D. Chisholm, A theoretical basis for the Lockhart–Martinelli correlation for two-phase flow, Int. J. Heat Mass Transf. 10 (1967) 1767–1778.
[21] L. Friedel, Improved friction pressure drop correlations for horizontal and vertical two-phase flow, The European Two-Phase Flow Group Meeting, Ispra, Italy, 1979.
[22] H. Müller-Steinhagen, K. Heck, A simple friction pressure drop correlation for two-phase flow in pipes, Che. Eng. Process. 20 (1986) 297–308.
[23] B.M. Fronk, S. Garimella, Heat transfer and pressure drop during condensation of ammonia in microchannels, in: the 3rd ASME International Conference on Micro/Nanoscale Heat and Mass Transfer, Atlanta, America, 2012.
[24] M.M. Shah, A general correlation for heat transfer during film condensation inside pipes, Int. J. Heat Mass Transf. 22 (1979) 547–556.
[25] K.W. Moser, R.L. Webb, B. Na, A new equivalent Reynolds number model for condensation in smooth tubes, ASME J. Heat Transf. 120 (1998) 410–417.
[26] K. Nilpueng, S. Wongwises, Two-phase gas-liquid flow characteristics inside a plate heat exchanger, Exp. Therm. Fluid Sci. 34 (2010) 1217–1229.
[27] C. Tribbe, H.M. Müller-Steinhagen, Gas/liquid flow in plate-and-frame heat exchangers - part II: two-phase multiplier and flow pattern analysis, Heat Transf. Eng. 22 (2001) 12–21.
[28] D. Winkelmann, Condensation of pure refrigerants and their zeotropic mixtures in plate heat exchangers. Ph.D. thesis, Commissiariat à l'energie atomique (CEA) (2010).
[29] V.G. Nino, P.S. Hrnjak, T.A. Newell, Characterization of two-phase flow in microchannels, ACRC Report TR202, Air Conditioning and Refrigeration Center, University of Illinois, Urbana-Champaign, 2002 at.
[30] D.C. Adams, P.S. Hrnjak, T.A. Newell, Pressure drop and void fraction in microchannels using carbon dioxide, ammonia, and R245fa as refrigerants, ACRC Report TR221, Air Conditioning and Refrigeration Center, University of Illinois, Urbana-Champaign, 2003 at.
[31] X. Tao, J.A. Kirkenier, C.A Infante Ferreira, Condensation of NH3 within a plate heat exchanger of small diameter channel, the 6th ASME International Conference on Micro/Nanoscale Heat and Mass Transfer, 2019 paper 3920.
[32] E.W. Jassim, T.A. Newell, J.C. Chato, Refrigerant pressure drop in chevron and bumpy style flat plate heat exchangers, Exp. Therm. Fluid Sci. 30 (2006) 213–222.
[33] S.M. Zivi, Estimation of steady-state steam void-fraction by means of the principle of minimum entropy production, ASME J. Heat Transf. 86 (1964) 247–251.
[34] S.Z. Rouhani, E. Axelsson, Calculation of void volume fraction in the subcooled and quality boiling regions, Int. J. Heat Mass Transf. 13 (1970) 383–393.
[35] M.J. Wilson, J.C. Chato, T.A. Newell, A.G. Kireta, A Study of Refrigerant Pressure Drop and Void Fraction in Flattened Copper Tubes, International Refrigeration and Air Conditioning Conference., Purdue, America, 2000.
[36] K.A. Triplett, S.M. Ghiaasiaan, S.I. Abdel-Khalik, A. LeMouel, B.N. McCord, Gas–liquid two-phase flow in microchannels part II: void fraction and pressure drop, Int. J. Multiph. Flow. 25 (1999) 395–410.
[37] X. Tao, E. Dahlgren, C.A Infante Ferreira, Condensation Heat Transfer and Pressure Drop of NH3 And NH3/H2O Within a Plate Heat Exchanger, 25th IIR International Congress of Refrigeration, Montreal, Canada, 2019 paper 727.
[38] J. Hart, P.J. Hamersma, J.M. Fortuin, Correlations predicting frictional pressure drop and liquid holdup during horizontal gas-liquid pipe flow with a small liquid holdup, Int. J. Multiph. Flow. 15 (1989) 947–964.
[39] B.X. Wang, X.Z. Du, Study on laminar film-wise condensation for vapor flow in an inclined small/mini-diameter tube, Int. J. Heat Mass Transf. 43 (2000) 1859–1868.
[40] S. Mancin, D. Del Col, L. Rossetto, Condensation of superheated vapour of R410A and R407C inside plate heat exchangers: experimental results and simulation procedure, Int. J. Refrig. 35 (2012) 2003–2013.
[41] B. Thonon, A. Bontemps, Condensation of pure and mixture of hydrocarbons in a compact heat exchanger: experiments and modelling, Heat Transf. Eng. 23 (2002) 3–17.
[42] J. Zhang, M.R. Kærn, T. Ommen, B. Elmegaard, H. Fredrik, Condensation heat transfer and pressure drop characteristics of R134a, R1234ze (E), R245fa and R1233zd (E) in a plate heat exchanger, Int. J. Heat Mass Transf. 128 (2019) 136–149.
[43] K. Sarraf, S. Launay, G El Achkar, L Tadrist, Local vs global heat transfer and flow analysis of hydrocarbon complete condensation in plate heat exchanger based on infrared thermography, Int. J. Heat Mass Transf. 90 (2015) 878–893.
[44] M.K. Dobson, Heat transfer and flow regimes during condensation in horizontal tubes, ACRC Report TR57, Air Conditioning and Refrigeration Center, University of Illinois, Urbana-Champaign, 1994 at.
[45] T. Ahn, J. Moon, B. Bae, J. Jeong, B. Bae, B. Yun, An empirical model of the wetted wall fraction in separated flows of horizontal and inclined pipes, Chem. Eng. Sci. 178 (2018) 260–272.
[46] W. Nusselt, Die oberflachenkondensation des wasserdampfes, Z. Ver. D. Ing. 60 (1916) 541–546.
[47] J.W. Rose, Fundamentals of condensation heat transfer: laminar film condensation, JSME Int. J. Ser. 2 31 (1988) 357–375.
[48] G.A. Longo, Heat transfer and pressure drop during hydrocarbon refrigerant condensation inside a brazed plate heat exchanger, Int. J. Refrig. 33 (2010) 944–953.
[49] W. Kast, E.S. Gaddis, K. Wirth, J. Stichlmair, Pressure drop in single phase flow, in: P. Stephan, H. Martin, S. Kabelac, D. Mewes, M. Kind, K. Schaber (Eds.), VDI Heat Atlas, Springer, Dusseldorf, 2010, pp. 1055–1115. 2nd Edition.
[50] H.J. Lee, S.Y Lee, Pressure drop correlations for two-phase flow within horizontal rectangular channels with small heights, Int. J. Multiph. Flow. 27 (2001) 783–796.

[51] E. Ungar, J. Cornwell, Two-phase pressure drop of ammonia in small diameter horizontal tubes, in: AIAA 17th Aerospace Ground Testing Conference, Nashville, America, 1992.
[52] Y. Chen, K.S. Yang, Y.J. Chang, C.C. Wang, Two-phase pressure drop of air–water and R-410A in small horizontal tubes, Int. J. Multiph. Flow. 27 (2001) 1293–1299.
[53] Y.S. Muzychka, M.M. Awad, Asymptotic generalizations of the Lockhart—Martinelli method for two phase flows, ASME J. Fluid. Eng. 132 (2010) 031302.
[54] C. Tribbe, H.M. Müller-Steinhagen, Gas/liquid flow in plate-and-frame heat exchangers - part I: pressure drop measurements, Heat Transf. Eng. 22 (2001) 5–11.
[55] Lemmon E.W., Huber M.L., and McLinden M.O. (2013). NIST standard reference database 23: reference fluid thermodynamic and transport properties-REFPROP, version 9.1, national institute of standards and technology, standard reference data program, Gaithersburg.
[56] N.B. Vargaftik, B.N. Volkov, L.D. Voljak, International tables of the interfacial tension of water, J. Phys. Chem. Ref. Data. 12 (1983) 817–820.